Ballistic Mobility Model for QDD Simulation of Ultra-short Transistors

P. Aguirre and A. Schenk

Integrated Systems Laboratory, ETH Zürich, CH 8092 Zürich, Switzerland

Abstract

A local TCAD model of the ballistic mobility is proposed that can be used in quantum drift-diffusion (QDD) simulations. It can be combined with models for density gradient correction and source-to-drain tunneling (STDT). These quantum effects strongly affect the transfer characteristics of $In_{0.53}Ga_{0.47}As$ double-gate ultra-thin-body (DG UTB) FETs with ultra-short channels.

(Keywords: Ballistic Mobility, QDD, DG UTB FETs)

Introduction

As the length of transistor channels is scaled down into the range of a few nanometers, quantum [1] and ballistic effects [6] start to play a major role. Quantum transport (QT) solvers (e.g. [11]) can accurately simulate such devices, but they are computationally expensive and still not mature for industrial environments.

In Ref. [2] we used the QDD simulator Sentaurus-Device from Synopsys [3] to simulate STDT in $In_{0.53}Ga_{0.47}As$ DG UTB FETs with L_G ranging from 10 nm to 25 nm (see Fig. 1). In these simulations, electron-phonon scattering is almost negligible, so the ballistic QT solutions obtained with the solver QTx [11] were taken as references for our QDD simulations. Fig. 1 shows the $I_D V_{GS}$-characteristics [2], which exhibit a pronounced current overshoot after the onset of inversion due to the exclusive usage of a diffusive mobility (μ_d). Therefore, the aim of this work is to present a model of the ballistic mobility that is capable of reducing the QDD current values to match the QTx values. In contrast to the various ballistic mobility models suggested in literature [5]-[8], this work proposes a local variant where the ballistic velocity is a continuous function of the quasi-Fermi potential (QPF). This simple form is well-suited for the combination with QDD models. Its detailed derivation as well as alternative variants in terms of the carrier density will be discussed elsewhere [4].

Model Description

The first moment of the Boltzmann transport equation (BTE) in relaxation time approximation reads

$$\left(\mu_d^{-1} + \frac{m_e}{q} \vec{v} \cdot \nabla \right) \vec{v} = \nabla \psi_n, \qquad (1)$$
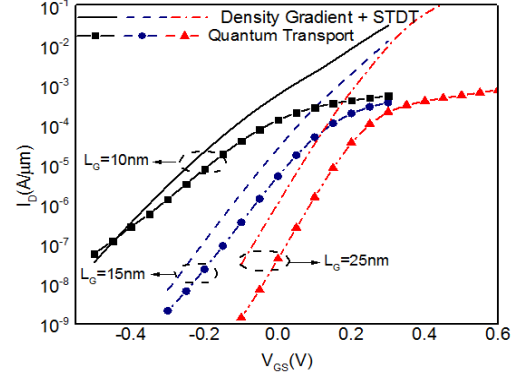

Fig. 1: $I_D V_{GS}$-characteristics obtained from the combination of QDD models with a constant diffusive mobility $\mu_d = 10^4 \frac{cm^2}{Vs}$ for an UTB FET with $t_{body} = 7$ nm and different gate lengths [2]. The ballistic reference curves were obtained with the QT solver QTx. $V_{DS} = 0.05$ V, $m_c = 0.0516\, m_0$.

where ψ_n is the QFP. In 1D (x-direction) one obtains

$$\frac{v}{\mu_d} + \frac{m_e}{q} v v' = \psi'_n. \qquad (2)$$

The second term starts to dominate if $\mu_d > q/(m_e |v'|) \approx q L_G / (m_e v_k(x_D))$ where $v_k(x_D)$ denotes the mean kinetic velocity at the end of the channel. In the kinetic limit, $\mu_d \to \infty$, Eq. (2) becomes an Euler equation, and integrating from the grounded source to the drain results in an energy balance equation for kinetic electrons:

$$v_k^2(x_D) - v_k^2(x_S) = \frac{2q}{m_e} \psi(x_D). \qquad (3)$$

In order to determine the mean kinetic velocity at the source, $v_k(x_S)$, it is assumed that electrons are injected from the S/D regions with the mean thermal velocity $v_{th} = \sqrt{kT/m_e}$. Neglecting scattering and counting only electrons with energies higher than the top of the STD barrier leads to

$$v_k(x_S) = v_{th} \frac{1 - e^{\frac{-q\psi(x_D)}{kT}}}{1 + e^{\frac{-q\psi(x_D)}{kT}}} = v_{th} \tanh(\frac{qV_{SD}}{2kT}). \qquad (4)$$

Inserting into Eq. (3) one obtains

$$v_k(x_D) = v_{th} \sqrt{\tanh^2(\frac{qV_{SD}}{2kT}) + \frac{2q\psi(x_D)}{kT}}. \qquad (5)$$

Note that both, $v_k(x_S)$ and $v_k(x_D)$, vanish at equilibrium ($V_{SD} = 0$ V) as required for *mean* velocities. The structure of Eq. (2) allows the definition of a ballistic mobility in the form:

$$\mu_b = \frac{q}{m_e} \frac{1}{v'_b} \xrightarrow[\mu_d \to \infty]{} \frac{v_k}{\psi'_n}. \qquad (6)$$

A model for a continuous ballistic velocity $v_b(x)$ is obtained if in Eq. (5) the dependence on x_D is replaced by the dependence on x:

$$v_b(x) = v_{th}\sqrt{\tanh^2(\frac{qV_{DS}}{2kT}) + \frac{2q\psi(x)}{kT}}. \qquad (7)$$

Note that this expression gives identical results for the mobility in Eq. (6), no matter if it is used for v_k or to compute v_b'. Therefore, we use the simple form

$$\mu_b(x) = \frac{v_b(x)}{\psi_n'(x)} \ . \qquad (8)$$

Implementation

The model (8) with (7) was implemented in the Physical Model Interface (PMI) HighFieldMobility of S-Device which combines the ballistic mobility model with the user-defined diffusive mobility by the Matthiessen rule. Eq. (8) was changed to $\mu_b(x) = \frac{v_b(x)}{|\nabla\psi_n|+\epsilon}$, where ϵ is an appropriate cutoff to avoid numerical instabilities. In a first step, the diffusive mobility μ_d was set to a large constant to mimic the ballistic regime and to allow comparisons with the QTx results when $\mu_b(x)$ is activated. The test device is an $In_{0.53}Ga_{0.47}$As DG

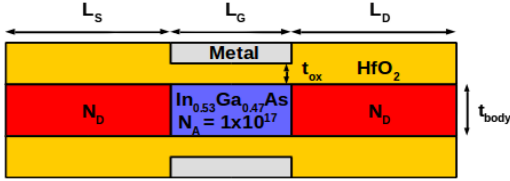Fig. 2: Schematic of simulated $In_{0.53}Ga_{0.47}$As DG UTB FET.

UTB FET (see Fig. 2) with L_G ranging from 7 nm to 15 nm. Body and oxide thicknesses, listed in Table I, where chosen according to assumed future technology nodes [9]. The effective transport mass m_e for each device was extracted from a QTx band structure simulation. Geometrical confinement leads to a certain shift of the threshold voltage (V_{th}) when the body thickness changes [10]. The shift found in QTx was modeled by a work function shift in S-Device. Another pronounced quantum effect in the studied short-channel FETs is STDT which shows up as leakage current in the sub-threshold regime. STDT was simulated in S-Device via the Nonlocal

TABLE I: Summary of dimensions, effective tunneling masses, and $V_{DS,sat}$ of the three simulated devices.

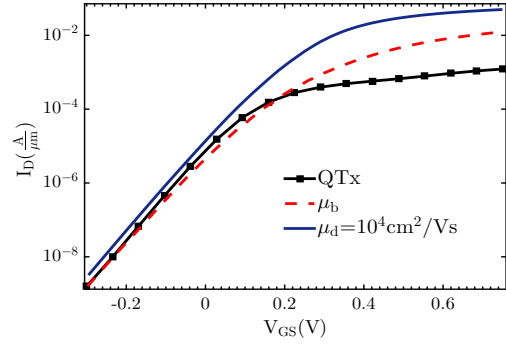| L_G	t_{body}	t_{ox}	m_e/m_0	$V_{DS,sat}$
7 nm	2.8 nm	2.6 nm	0.080	0.56 V
11.5 nm	4.6 nm	3.2 nm	0.0678	0.61 V
15 nm	7 nm	3.7 nm	0.0516	0.63 V

Fig. 3: $I_D V_{GS}$-characteristics of an $In_{0.53}Ga_{0.47}$As DG UTB FET (L_G=15 nm) computed with μ_b and with μ_d = 10^4 cm^2/Vs for V_{DS} = 0.05 V.
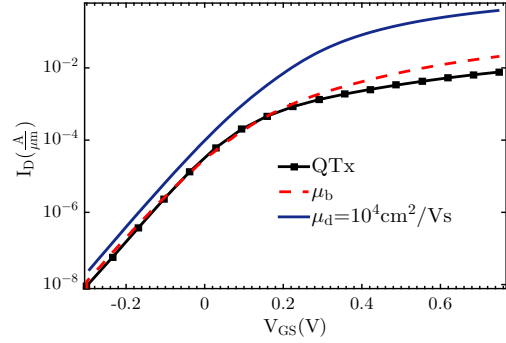

Fig. 4: Same as Fig. 3, but for V_{DS} = 0.63 V.

Tunneling (NLT) model [3] using the values m_e from Table I for the tunneling mass.

Results and Discussion

Fig. 3 presents the simulated $I_D V_{GS}$-curves for L_G = 15 nm, computed with $\mu_b(x)$ (Eq. (8)) and μ_d = 10^4 cm^2/Vs for V_{DS} = 0.05 V and Fig. 4 shows the corresponding curves for V_{DS} = 0.63 V. The QTx reference characteristics are plotted for comparison.

In Fig. 5 the simulated transfer characteristics for L_G=7 nm and L_G=11.5 nm computed with μ_b (Eq. (8)) are plotted for V_{DS} = 0.05 V and Fig. 6 shows the corresponding curves in the saturation regime ($V_{DS,sat}$ given in Table I). Extracted sub-threshold swing (SS) and on-current I_{ON} values
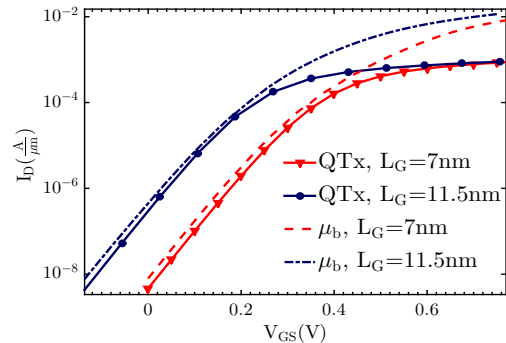

Fig. 5: $I_D V_{GS}$-characteristics of $In_{0.53}Ga_{0.47}$As DG UTB FETs (L_G=7 nm and L_G=11.5 nm), computed with μ_b for V_{DS} = 0.05 V.
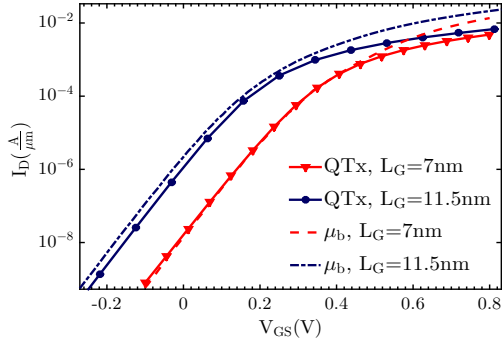
Fig. 6: Same as Fig. 5, but for L_G=7 nm at V_{DS} = 0.56 V and L_G=11.5 nm at V_{DS} = 0.61 V.

TABLE II: Summary of SS and I_{on} extracted at V_{GS}=0.68 V and V_{DS} = 0.05 V for different L_G.

L_G	QTx SS($\frac{mV}{dec}$)	QDD SS($\frac{mV}{dec}$)	QTx $I_{on}(\frac{A}{\mu m})$	QDD $I_{on}(\frac{A}{\mu m})$
7 nm	78	79.5	7.4E-4	50E-4
11.5 nm	74	76	8.1E-4	93E-4
15 nm	81.2	86.6	10E-4	100E-4

TABLE III: Same as Table II, but for L_G=7 nm at V_{DS} = 0.56 V, L_G=11.5 nm at V_{DS} = 0.61 V and L_G=15 nm at V_{DS} = 0.63 V.

L_G	QTx SS($\frac{mV}{dec}$)	QDD SS($\frac{mV}{dec}$)	QTx $I_{on}(\frac{A}{\mu m})$	QDD $I_{on}(\frac{A}{\mu m})$
7 nm	81	83	32E-4	74E-4
11.5 nm	75	75.4	50E-4	142E-4
15 nm	82	90	64E-4	167E-4

from the QTx reference simulations and the QDD simulations of all the studied devices are summarized in Table II for V_{DS}=0.05 V and in Table III for the different values of $V_{DS,sat}$. The non-monotonous trend for SS is caused by the assumed thickness of the gate oxide in combination with the changing body thickness, which leads to variations in the electrostatic control. The proposed model of the ballistic mobility in combination with the S-Device default model of STDT (Nonlocal Tunneling) is able to reproduce the QTx transfer characteristics in the sub-threshold regime at low and high V_{DS} (see Figs. (5) and (6)). However, after the onset of inversion the QDD current is still overestimated compared to QTx. The discrepancy is quite strong in the linear regime, but much smaller in the saturation regime. This can be traced back to the shape of the QFP $\psi_n(x)$ which is plotted in Fig. 7 for both source-drain bias conditions and V_{GS} = 0.42 V (after the onset of inversion). At high drain bias,

the shape of the QFP is more like a smoothed step function, i.e. very close to the case of the kinetic transport regime where it is exactly a step function
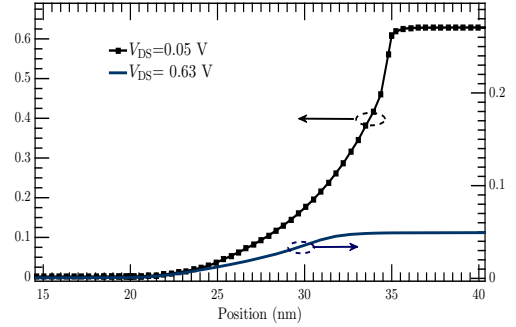

Fig. 7: Quasi-Fermi potential $\psi(x)$ of an $In_{0.53}Ga_{0.47}As$ DG UTB FET (t_{body} = 7 nm, L_G =15 nm) at V_{GS}=0.42 V (after the onset of inversion) in the linear (V_{DS} = 0.05 V) and saturation regime (V_{DS} = 0.63 V).

(electrons keep their QFP from the contacts). Note, that this had been the initial assumption to construct the model for the ballistic velocity. In the linear regime, the channel becomes a low-Ohmic resistor with an almost linear $\psi_n(x)$, a situation furthest from the kinetic transport regime. This behaviour calls for improvements in modelling the ballistic velocity.

References
[1] A. Wettstein et al., IEEE T-ED, vol. 48, pp. 279-284, 2001. [2] P. Aguirre et al., Proceedings SISPAD, pp. 53-56, 2016. [3] Sentaurus Device User Guide, V-2015.06, Synopsys Inc., 2015. [4] A. Schenk and P. Aguirre, to be published in IEEE T-ED. [5] M. S. Shur, IEEE Trans. On electron Device Letters, vol. 23 (9), pp. 511-513, 2002. [6] M. Lundstrom et al., arXiv:1603.03132, 2016. [7] W. R. Frensley, IEEE T-ED, vol. 30 (12), pp. 1619-1623, 1983. [8] R. Kotlyar et al., IEE T-ED, vol. 62 (3), pp. 743-750, 2015. [9] Extended Intel Technology Road Map, private communication with IMEC, see also www.iii-v-mos-project.eu [10] A. Schenk et al., Proceedings SISPAD, pp. 552-555, 2002. [11] M. Luisier et al., Jour. Appl. Phys., vol. 100 (4), 2006.